Journal Pre-proof

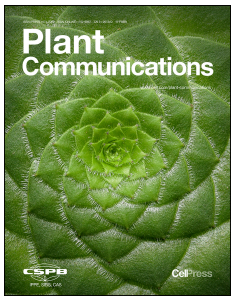

OsBRK1-mediated phosphorylation of OsPFN2 regulates meiotic spindle actin assembly and rice fertility

Hai Zheng, Zhigang Zhao, Shanshan Zhu, Yulong Ren, Jiangfeng Shen, Ziqi Xun, Xiaowen Yu, Chaolong Wang, Bowen Yao, Siqi Cheng, Yang Hu, Shihao Zhang, Qiming Wang, Jiayu Lu, Zhenwei Xie, Dekun Lei, Anqi Jian, Minrui Chen, Keyi Chen, Shijia Liu, Xi Liu, Yunlu Tian, Lin Jiang, Zhijun Cheng, Cailin Lei, Qibing Lin, Xiupin Guo, Xin Wang, Chuanyin Wu, Haiyang Wang, Shanjin Huang, Jianmin Wan

PII: S2590-3462(25)00179-8

DOI: https://doi.org/10.1016/j.xplc.2025.101417

Reference: XPLC 101417

To appear in: *PLANT COMMUNICATIONS*

Received Date: 13 December 2024

Revised Date: 5 May 2025

Accepted Date: 9 June 2025

Please cite this article as: Zheng, H., Zhao, Z., Zhu, S., Ren, Y., Shen, J., Xun, Z., Yu, X., Wang, C., Yao, B., Cheng, S., Hu, Y., Zhang, S., Wang, Q., Lu, J., Xie, Z., Lei, D., Jian, A., Chen, M., Chen, K., Liu, S., Liu, X., Tian, Y., Jiang, L., Cheng, Z., Lei, C., Lin, Q., Guo, X., Wang, X., Wu, C., Wang, H., Huang, S., Wan, J., OsBRK1-mediated phosphorylation of OsPFN2 regulates meiotic spindle actin assembly and rice fertility, *PLANT COMMUNICATIONS* (2025), doi: https://doi.org/10.1016/j.xplc.2025.101417.

OsBRK1-mediated phosphorylation of OsPFN2 regulates meiotic spindle actin assembly and rice fertility

Hai Zheng[1,4], Zhigang Zhao[2,4], Shanshan Zhu[1,4], Yulong Ren[1], Jiangfeng Shen[3], Ziqi Xun[1], Xiaowen Yu[2], Chaolong Wang[2], Bowen Yao[2], Siqi Cheng[2], Yang Hu[2], Shihao Zhang[2], Qiming Wang[2], Jiayu Lu[2], Zhenwei Xie[2], Dekun Lei[2], Anqi Jian[2], Minrui Chen[2], Keyi Chen[2], Shijia Liu[2], Xi Liu[2], Yunlu Tian[2], Lin Jiang[2], Zhijun Cheng[1], Cailin Lei[1], Qibing Lin[1], Xiupin Guo[1], Xin Wang[1], Chuanyin Wu[1], Haiyang Wang[1], Shanjin Huang[3,*] and Jianmin Wan[1,2,*]

[1]State Key Laboratory of Crop Gene Resources and Breeding, National Key Facility for Crop Gene Resources and Genetic Improvement, Institute of Crop Sciences, Chinese Academy of Agricultural Sciences, Beijing 100081, China.

[2]State Key Laboratory of Crop Genetics & Germplasm Enhancement and Utilization, Nanjing Agricultural University, Nanjing 210095, China.

[3]Center for Plant Biology, School of Life Sciences, Tsinghua University, Beijing 100081, China.

[4]These authors contributed equally to this work

[*]Correspondence: Jianmin Wan (wanjianmin@caas.cn) and Shanjin Huang (sjhuang@tsinghua.edu.cn).

Running title: OsBRK1 regulates spindle actin assembly by phosphorylating OsPFN2

Short Summary: We demonstrate that OsPFN2-OsRMD module is involved in spindle actin assembly in rice PMCs and OsBRK1 regulates spindle actin assembly by phosphorylating OsPFN2 that determines the availability of OsRMD utilizable actin-OsPFN2 complexes.

Abstract

The formation of a meiotic spindle structure is crucial for chromosome segregation and fertility in plants. Previous studies have shown that actin decorates spindle microtubules in mammalian oocytes, forming spindle actin, which is indispensable for genome stability and gamete segregation. However, the regulatory mechanisms underlying spindle actin assembly remain unknown. Here, we report that dysfunction of OsPFN2, a rice profilin protein, disrupts meiotic spindle actin assembly and spindle microtubule structure, and causes errors in chromosome alignment and segregation in pollen mother cells (PMCs), resulting in male sterility. Furthermore, our results demonstrate that OsPFN2 interacts with Rice Morphology Determinant (OsRMD), a formin protein in rice, whose depletion also impacts spindle actin assembly and meiotic spindle microtubule structure. Intriguingly, we identified an interaction between OsPFN2 and Bub1-Related Kinase 1 (OsBRK1) and demonstrated that OsBRK1 depletion enhances spindle actin assembly. Additionally, we found that OsBRK1 phosphorylates OsPFN2, and the resulting phospho-mimetic OsPFN2 retains its capability to bind actin. However, these phospho-mimetic actin-OsPFN2 complexes are not utilized by OsRMD. Our findings thus reveal that the OsPFN2-OsRMD module controls meiotic spindle actin assembly, and OsBRK1 fine-tunes this process through phosphorylation of OsPFN2.

Keywords: Rice (*Oryza sativa*), spindle actin assembly, spindle morphogenesis, pollen development, male sterile

Introduction

The process of pollen development in angiosperms is a critical biological event with significant implications for plant reproduction (Zhang et al., 2011). The process includes specialized cell cycle that employs a reductional cell division to produce haploid gametes during meiosis, and then returning to the original ploidy level during fertilization (Mercier et al., 2015; He et al., 2016; Xue et al., 2019). During the two cell divisions of meiosis, accurate chromosome attachment and segregation movement are

crucial for transmission of genetic information, which strictly relies on the formation of proper spindle that is a complex microtubule-based structure (Schuh and Ellenberg, 2008; Liu et al., 2011; McMichael and Bednarek, 2013; Holubcová et al., 2015; Lee and Liu, 2019). Dysfunction of spindle structure often leads to erroneous alignment and segregation of chromosomes, resulting in aneuploidy with catastrophic consequences on pollen development, leads to sterility (Lee et al., 2015; Mercier et al., 2015; Ullrich et al., 2019; Xue et al., 2019). Despite the identification of several genes, including *OsMTOPVIB*, *OsPRD1*, *AtMPS1*, *OsPSS1* and *AtATK1*, as being implicated in the regulation of spindle morphogenesis in PMCs (Chen et al., 2002; Jiang et al., 2009; Zhou et al., 2011; Xue et al., 2019; Shi et al., 2021; Zhou et al., 2024), the precise mechanisms underlying spindle morphogenesis in PMCs remain largely unknown.

The actin cytoskeleton has been implicated in the regulation of microsporogenesis and male gametophyte development in plants. For instance, suppression of expression of genes encoding actin bundlers, *PLIM2a*, *PLIM2b* and *PLIM2c*, through RNA interference disrupts pollen development, resulting in complete male sterile (Ye and Xu, 2012). Similarly, overexpression of Maize *actin depolymerizing factor 1* (*ZmADF1*) in *Arabidopsis* leads to a significant reduction in pollen grain number (Lv et al., 2024). Intriguingly, recent studies have shown that actin is an integral component of the meiotic spindle in mammals, *Drosophila* and humans, forming a structure resembling spindle microtubules and termed spindle actin (Sheykhani et al., 2013; Mogessie and Schuh, 2017; Roeles and Tsiavaliaris, 2019; Dunkley and Mogessie, 2023; Wood et al., 2024). Spindle actin is indispensable for genome stability and gamete segregation. Although spindle shaped actin filament structures have been observed in PMCs of maize and wheat (Staiger and Cande, 1991; Xu et al., 2013), whether it is equivalent to spindle actin reported in mammalian oocytes remains unknown. In addition, the specific function of these spindle shaped actin filaments remains uncharacterized in plants. Previous actin-based pharmacological treatments to either reduce or increase the amount of spindle actin result in the formation of disorganized meiotic spindles, leading to abnormal chromosome behavior in mouse, *Drosophila* and human oocytes (Mogessie and Schuh, 2017; Roeles and

Tsiavaliaris, 2019; Wood et al., 2024). These findings demonstrate that spindle actin plays a crucial role in regulating spindle morphogenesis. However, to date, the mechanism regulating the assembly and disassembly of spindle actin remains unknown.

Formin, an actin nucleation and elongation factor (Courtemanche, 2018), has been implicated in the regulation of spindle actin assembly. Specifically, studies have demonstrated that the loss of function of *FORMIN-2* (*FMN2*) in mouse or its homologue gene, *Cappuccino* (*Capu*), in *Drosophila* results in a reduction of spindle actin, leading to abnormal chromosome behavior in oocytes (Mogessie and Schuh, 2017; Wood et al., 2024). Despite the implication of formin in the regulation of pollen fertility, as evidenced by mutations in *Rice Morphology Determinant* (*OsRMD*, rice *formin 5*) and *Dwarf and Reduced Tillering 1* (*OsDRT1*, rice *formin 13*), which lead to decreased pollen fertility in rice (Li et al., 2018; Zhang et al., 2023), and mutation in *Arabidopsis Formin 14* (*AtFH14*) that has a deleterious effect on microtubule arrangement and results in defective microspore formation (Li et al., 2010), direct evidence linking formin to spindle actin assembly remains lacking. Given that profilin, an actin monomer binding protein, and formin function as a module to regulate actin polymerization (Kovar, 2006; Cao et al., 2016; Henty-Ridilla et al., 2017; Sun et al., 2018), as demonstrated in pollen (Liu et al., 2015; Liu et al., 2021), functional characterization of profilin during meiosis will offer insights into the mechanisms by which the profilin-formin module controls spindle actin assembly.

Prior to successful segregation, chromosomes must attach to spindle microtubules, a process monitored by the mechanism called spindle assembly checkpoint (SAC) to ensure sensitive, responsive, and robust attachment (Musacchio and Salmon, 2007; Lampson and Cheeseman., 2011; Akera et al., 2017; McAinsh and Kops, 2023). Several conserved proteins, including budding uninhibited by benzimidazole 1 (Bub1), monopolar spindles 1 (Mps1), Bub3, mitotic arrest-deficient protein 1 (Mad1), Mad2, and Mad3/BubR1, cooperate to mediate SAC function (Kim et al., 2012; London and Biggins, 2014; Ji et al., 2015; Touati and Wassmann, 2016; Zhang et al., 2018; Deng et al., 2024). Phosphorylation/dephosphorylation events mediated by these SAC proteins constitute major signaling events within SAC mechanisms. Bub1 encodes a Ser/Thr

protein kinase that is not only required for the centromeric localization of Cenp-F, BubR1, Cenp-E, and Mad2, but is also essential for the phosphorylation of Histone H2A and the centromeric localization of shugoshin (Kitajima et al., 2004; Wang et al., 2012). In rice, OsBRK1, a homolog of Bub1, is required for correcting improper attachment of paired sister kinetochores (Wang et al., 2012). However, as OsBRK1 lacks the Gle2 domain and KEN box that are critical for SAC function, it was presumed to have lost its classical SAC roles. Consequently, the molecular mechanism by which OsBRK1 controls meiosis in plants remains to be elucidated (Komaki and Schnittger, 2016). In addition, the levels of Bub1 at the kinetochore underwent a rapid decrease at the inception of anaphase in mouse and human oocytes (Yin et al., 2006; Lagirand-Cantaloube et al., 2017). In contrast, OsBRK1 was deemed a stable component of the kinetochore-associated proteins throughout both meiotic stages (Wang et al., 2012). Analogously, previous studies revealed that fission yeast Bub1 remains associated with the kinetochore throughout the entire meiotic process, hinting at potential additional roles for OsBRK1 in regulating spindle-based functions (Bernard et al., 2001). Consequently, these observations underscore the necessity for further investigation into whether OsBRK1 participates in additional, as yet uncharacterized mechanisms regulating meiosis.

In this study, we demonstrate that actin decorates spindle microtubules and forms spindle actin structures in rice PMCs. By analyzing mutants of *OsPFN2* and *OsRMD* in rice, we show that the profilin-formin module plays a crucial role in controlling spindle actin assembly during meiosis in PMCs. Intriguingly, we further demonstrate that OsBRK1 is involved in regulating spindle actin assembly through phosphorylation of OsPFN2, which in turn controls the availability of formin-utilizable actin-profilin complexes to drive spindle actin assembly. Collectively, our findings provide insights into the molecular mechanisms governing meiotic spindle actin assembly and its regulatory process in plants.

Results

Formation of spindle actin in rice PMCs

To investigate the role of actin during meiosis in plants, we visualized the distribution of actin filaments in PMCs and their spatial relationship with spindle microtubules. Specifically, we examined the filamentous actin (F-actin) structure, both independently and in conjunction with microtubules in wild type (WT) rice PMCs. The results showed that actin filaments were distributed evenly in the cytoplasm from diakinesis to dyad, and the F-actin formed a barrel-shaped spindle structure from metaphase I to anaphase I (Supplemental Figure 1A; Supplemental Movie 1-3). Subsequently, new F-actin was seen between the segregated chromosomes at the telophase I stage and the barrel-shaped F-actin gradually vanished at the dyad stage (Supplemental Figure 1A; Supplemental Movie 4, 5). The actin filaments distributed uniformly in the cytoplasm are classified as cytoplasmic actin, while the actin filaments forming barrel-shaped spindle structure are called spindle actin (Figure 1, A-C; Supplemental Figure 1A). By direct visualization of both actin filaments and microtubules simultaneously, we found that they tightly associated with each other on the spindle during meiosis (Figure 1, A-C; Supplemental Figure 1B). These results suggest that actin is an integral component of the spindle, which may be required for functional integrity of the spindle.

Dysfunction of OsPFN2 leads to male sterile and abnormal chromosome behavior

To explore the role of spindle actin in rice PMCs, we initially focused on characterizing profilin, which is an essential actin regulatory protein and constitutes a small gene family of three members in rice. *OsPFN1.1* (*LOC_Os10g17660*) and *OsPFN1.2* (*LOC_Os10g17680*) exhibit stage-specific expression during late pollen development, whereas *OsPFN2* (*LOC_Os06g05880*) is ubiquitously expressed in all analyzed tissues, with elevated transcript levels detected from meiosis to pollen maturation (Supplemental Figure 2, A-H). Since *OsPFN2*, but not *OsPFN1.1* and *OsPFN1.2*, is highly expressed in meiotic anthers, we hypothesized that *OsPFN2* might be involved in the regulation of spindle actin assembly during meiosis. To investigate a possible role of OsPFN2 in regulating spindle actin assembly in PMCs, we employed the CRISPR/Cas9-mediated genome editing technology to edit *OsPFN2* gene. Two allelic

mutants were obtained for *OsPFN2*: *Ospfn2-1* with 3-bp deletion (results in the deletion of Methionine at 12th amino acid of OsPFN2) and *Ospfn2-2* with 3-bp deletion and 1-bp insertion (Figure 2, A and B). The results of pollen staining assay showed that *Ospfn2-1* and *Ospfn2-2* were male-sterile (Figure 2C). Heterozygous *Ospfn2-1* seeds were successfully obtained through WT pollen fertilization, whereas *Ospfn2-2* alleles failed to produce viable heterozygous seeds via this method. Homozygous *Ospfn2-1* plants derived from these seeds were subsequently used for phenotypic characterization. Phenotypic observation revealed that, in addition to pollen sterility, the *Ospfn2-1* mutant displayed a significant reduction in plant height (Figure 2, D-F). To characterize *Ospfn2-1* for the pollen abortion, we observed detailed structural changes by anther cross-section and transmission electron microscopy (TEM). We found that the dysfunction of OsPFN2 caused shriveled anthers and delayed tapetum degradation (Supplemental Figure 3, A and B). Abnormal tapetum degradation further resulted in defective pollen exine formation (Supplemental Figure 3C). Microscopic analysis revealed that *Ospfn2-1* plants developed morphologically normal embryo sacs (Figure 2, D and G). These observations indicate that in the *Ospfn2-1* mutant, pollen development is specifically impaired, while the formation of the embryo sac is not affected, highlighting a key role for OsPFN2 in male reproductive tissues. DAPI staining of the *Ospfn2-1* PMCs further revealed meiotic defects, including chromosome misalignment and aberrant segregation during meiosis I (Figure 2, H and I). Despite these segregation errors, bivalents at the diakinesis stage exhibited normal morphology (Figure 2H), indicating that OsPFN2 dysfunction does not impair chromosome pairing or synapsis. This observation suggests a defect in chromosome segregation dynamics during meiosis I, thereby prompting our subsequent efforts to functionally characterize the role of OsPFN2 in meiotic chromosome behavior.

Dysfunction of OsPFN2 leads to the formation of defective spindle actin

Given that OsPFN2 is a typical profilin family protein that binds to actin monomers and inhibits spontaneous actin polymerization, we investigate how dysfunction of OsPFN2 affects the spindle actin cytoskeleton in PMCs. We found that the spindle actin

density was decreased in *Ospfn2-1*, compared to the WT (Figure 3, A and B). Furthermore, the spindle in *Ospfn2-1* PMC was found to be loosely structured, as evidenced by a reduction in spindle length and an increase in spindle width (Figure 3, C-G). Together, these results suggest that OsPFN2 plays a key role in maintaining the amount of spindle actin, which is essential for ensuring the structural and functional integrity of the meiotic spindle (Supplemental Figure 4).

OsBRK1 interacts with OsPFN2 and loss of function of OsBRK1 increases the density of spindle actin and alters the shape of meiotic spindle

Next, we found that, OsPFN2 is localized uniformly to the cytosol during meiosis I (Figure 4A), which is similar to the findings in *Arabidopsis* pollen tube (Liu et al., 2015). To explore the regulatory role of uniformly distributed OsPFN2 in spindle actin assembly in PMCs, we conducted a yeast two-hybrid (Y2H) screen using OsPFN2 as a bait against a rice meiosis anther yeast library (Supplemental Table 1). Intriguingly, we identified OsBRK1, a serine/threonine protein kinase homologous to yeast Bub1, as an interacting partner of OsPFN2. Notably, Bub1, previously characterized as a key SAC protein, is involved in monitoring chromosome attachment to spindle (Klebig et al., 2009; Kawashima et al., 2010; Musacchio, 2015; Sacristan and Kops, 2015; Vleugel et al., 2015; Komaki and Schnittger, 2016). Further Y2H, bimolecular fluorescence complementation (BiFC) and co-immunoprecipitation (Co-IP) assays confirmed that OsPFN2 indeed interacts with OsBRK1 (Figure 4, B-D). Earlier studies have shown that kinetochore-localized OsBRK1 is required for correcting the improper attachment of paired sister kinetochores (Wang et al., 2012). We reasoned that OsBRK1 might have impact on meiotic spindle actin assembly through its interaction with OsPFN2 near kinetochores. To verify a role of OsBRK1 in spindle actin assembly in rice PMCs, we generated mutant of *OsBRK1* using the CRISPR/Cas9 technology (Supplemental Figure 5A). Cellular examination revealed that the *Osbrk1* mutant which exhibited meiotic spindle actin and spindle microtubule defects, as evidenced by the narrower and longer spindle with increased spindle actin density (Figure 4, E-I). Together, these results demonstrate that kinetochore-localized OsBRK1 is involved in the regulation of

spindle actin assembly and spindle morphogenesis.

OsBRK1 phosphorylates OsPFN2

To investigate whether OsBRK1 phosphorylates OsPFN2, a phosphorylation experiment was performed *in vitro*. The results demonstrated that purified recombinant MBP-tagged OsBRK1 protein effectively phosphorylated His-tagged OsPFN2 protein (Figure 5A). To identify the specific residues in OsPFN2 that are targets of OsBRK1, liquid chromatography-tandem mass spectrometry (LC-MS/MS) analysis was performed. This analysis revealed three phospho-peptides with phosphorylation occurring at three residues Thr21, Thr97 and Ser100 (Supplemental Figure 6). To further confirm that these residues are indeed phosphorylated by OsBRK1, site-directed mutagenesis was performed, substituting Thr21, Thr97, and Ser100 with non-phosphorylatable Alanine (Ala). Subsequent phosphorylation assays showed that substitution of these three residues all caused a significant reduction in the phosphorylation level of OsPFN2 mediated by OsBRK1 (Figure 5B). These findings indicate that Thr21, Thr97 and Ser100 are *bona fide* phosphorylation sites in OsPFN2 targeted by OsBRK1.

The phospho-mimetic OsPFN2s retain the ability to interact with actin and non-phosphorylatable OsPFN2s fail to rescue spindle actin defects in *Ospfn2-1*

Next, we initially determined how OsBRK1-mediated phosphorylation alters the ability of OsPFN2 to interact with actin. By performing actin polymerization assay, we found that phospho-mimetic OsPFN2^{T21D}, OsPFN2^{T97D} and OsPFN2^{S100D} retained roughly the same capability in inhibiting spontaneous actin assembly as OsPFN2^{WT} (Figure 5C), suggesting that the phosphorylation of OsPFN2 by OsBRK1 does not alter its binding capacity to actin. To uncover the biological relevance of phosphorylation of OsPFN2 *in vivo*, we generated three versions of mutated *OsPFN2* containing T21A, T97A and S100A substitution, respectively, and transformed them into the *Ospfn2-1* background. As expected, the *OsPFN2:gOsPFN2^{WT}* transgene restored pollen fertility, spindle actin density and spindle morphology of the *Ospfn2-1* mutant. By comparison, the mutant

transgenes partially restored the pollen fertility, spindle actin density and spindle morphology of *Ospfn2-1*, and the incomplete restoration of these phenotypes in *Ospfn2-1* is not attributed to variations in the levels of gene expression (Figure 5, D-K). These results suggests that OsBRK1-mediated regulation of OsPFN2 is biologically significant in spindle actin assembly. To further elucidate the genetic relationship between OsBRK1 and OsPFN2, we generated an *Ospfn2-1Osbrk1* double mutant using CRISPR/Cas9-mediated genome editing. Phenotypic analysis revealed that this double mutant exhibited disrupted spindle actin assembly, mirroring the defects observed in the *Ospfn2-1* single mutant (Supplemental Figure. 7). Collectively, these results support a model wherein OsBRK1 acts upstream of OsPFN2 to regulate spindle actin assembly.

OsRMD and OsPFN2 form a module that facilitates the assembly of spindle actin

Given that formin proteins utilize actin-profilin complexes to facilitate actin polymerization (Li et al., 2010; Yang et al., 2011; Sun et al., 2013; Liu et al., 2015), prompts speculation that OsBRK1-mediated phosphorylation of OsPFN2 may disrupt the formin function in driving spindle actin assembly in PMCs. Previous studies have established OsRMD as a critical actin nucleation factor regulating diverse developmental processes, such as rice vegetative morphogenesis and pollen tube elongation (Yang et al., 2011; Zhang et al., 2011; Li et al., 2018). Its functional conservation in actin dynamics prompted us to investigate its potential involvement in meiotic spindle regulation. To demonstrate this, we generated the *Osrmd* mutant using CRISPR/Cas9-mediated gene editing, which exhibits a significant reduction in pollen fertility (Supplemental Figure 5, B and C). By directly visualizing spindle actin in rice PMCs, we found that the spindle actin density in the *Osrmd* mutant was decreased compared to that of WT (Figure 6, A and B). Furthermore, the spindle is loosely structured in the *Osrmd* mutant (reduced length) compared to that in WT (Figure 6, C-E). These data suggest that OsRMD is required for the generation of spindle actin in rice PMCs.

Next, by performing Y2H, BiFC and Co-IP experiments, we demonstrated that

OsRMD strongly interacted with OsPFN2 (Supplemental Figure 8, A-C). Additionally, we demonstrated that OsRMD FH1FH2 (containing the truncated FH1 domain and full-length FH2 domain) is able to overcome the inhibitory effect of OsPFN2 on actin nucleation and accelerates actin polymerization (Figure 6F), these results suggests that OsPFN2 and OsRMD synergistically promote actin assembly. Consistent with prior reports that OsRMD binds and bundles both F-actin and microtubules *in vitro* (Yang et al., 2011; Zhang et al., 2011), our *in vivo* colocalization studies using *Nicotiana benthamiana* leaf epidermal cells co-expressing GFP-OsRMD, MAP65-RFP (microtubule marker), and FABD2-CFP (F-actin marker) revealed that OsRMD associates with both cytoskeletal elements (Supplemental Figure 9). Collectively, these findings lead us to propose that OsRMD and OsPFN2 cooperate as a functional module to promote spindle-associated actin assembly, ensuring proper spindle morphogenesis and functional integrity during PMC meiosis.

Phosphorylation of OsPFN2 attenuates the capability of OsRMD in utilizing actin-OsPFN2 complexes to nucleate actin assembly

To understand how OsBRK1-mediated phosphorylation of OsPFN2 impacts the function of OsRMD in spindle actin assembly, we performed the *in vitro* actin polymerization experiments. The results showed that OsRMD FH1FH2 had reduced activity in utilizing phosphomimetic actin-OsPFN2^{T21D}, actin-OsPFN2^{T97D}, or actin-OsPFN2^{S100D} complexes in promoting actin polymerization (Figure 6F). This observation suggests that the compromised function of OsPFN2^{T21D}, OsPFN2^{T97D} and OsPFN2^{S100D} in spindle actin assembly likely due to the formation of actin-profilin complexes unavailable to formin. In agreement with this, we found that the binding affinity of phosphomimetic OsPFN2^{T21D}, OsPFN2^{T97D} and OsPFN2^{S100D} to OsRMD decreased when compared to OsPFN2^{WT} by split-luciferase complementation assay and semi-*vivo* protein interaction assay in *Nicotiana benthamiana* (Figure 6, G and H; Supplemental Figure 10). These results suggest that OsBRK1-mediated phosphorylation of OsPFN2 leads to the formation of phosphorylated actin-OsPFN2 complexes, which modulates functionality level of the profilin (OsPFN2)-formin

(OsRMD) module to regulate the accurate formation of spindle actin and spindle microtubules during meiosis.

Discussion

Although an essential role of spindle microtubule in proper chromosome attachment and segregation during mitosis and meiosis is well documented (Musacchio and Salmon, 2007; Liu and Lee, 2022), a role of spindle actin in these processes has only recently begun to emerge. Here, we provide evidence that spindle actin is an integral component of the spindle in rice. In addition, our results show that spindle actin is essential for the proper formation of spindle microtubule, and that proper assembly and regulation of both spindle filaments are required for accurate alignment and segregation of chromosomes during meiosis. Intriguingly, we demonstrate that OsBRK1, a homologous protein of the SAC core kinase Bub1, monitors spindle actin assembly via phosphorylating OsPFN2 to fine-tune the availability of actin-OsPFN2 complexes readily usable by OsRMD during meiosis, which is essential for spindle morphogenesis in rice (Figure 7).

Our results have several important implications. First, our study, along with the researches on mammalian and *Drosophila* oocytes (Mogessie and Schuh, 2017; Roeles and Tsiavaliaris, 2019; Dunkley and Mogessie, 2023; Wood et al., 2024), demonstrates that spindle actin is an integral component of the spindle apparatus. This component is crucial for the accurate formation and functional integrity of meiotic spindle in both plants and animals. OsPFN2-OsRMD-mediated spindle actin assembly, acts like a scaffold, playing a key role in supporting the structural stability of meiotic spindle microtubules. In support of this notion, OsPFN2^{-M} (refers to the one Methionine deletion of OsPFN2 in *Ospfn2-1* mutant) has reduced activity in promoting actin polymerization that fails to support spindle actin assembly leading to destabilization of spindle microtubule structure (Supplemental Figure 4 and Supplemental Figure 11). Therefore, we propose that the regulation of spindle actin represents an additional layer of control over meiotic spindle stability and function, complementing the role of spindle microtubules. This additional regulation is believed to increase the accuracy and

efficiency of meiotic spindle function and reduce the risk of aneuploidy. Secondly, our findings suggest that profilin and formin interact with each other and they form a functional module during the assembly process of spindle actin in rice PMCs. Together with the earlier reports that depletion of formin impairs spindle actin assembly in oocytes (Mogessie and Schuh, 2017), we speculate that meiotic spindle actin assembly mediated by the profilin-formin module might be a universal mechanism. Thirdly, our findings that the activity of profilin-formin in spindle actin assembly is regulated by kinetochore-localized OsBRK1 (Figure 7), suggest that the profilin-formin module likely function near kinetochore during meiotic spindle actin assembly. Consistently, it has been reported that formin family proteins, including OsRMD, AtFH14 and FMN2, interact with both microtubules and actin filaments (Li et al., 2010; Zhang et al., 2011; Mogessie and Schuh, 2017). Thus, these observations suggest that formins may bind to spindle microtubules to nucleate spindle actin assembly during meiosis. This hypothesis remains to be an interesting avenue worthy of further investigations in the future.

An interesting finding of this study is that OsBRK1 plays an important role in fine-tuning spindle actin assembly by mediating the phosphorylation of OsPFN2, thus regulating the availability of formin-utilizable actin-profilin complexes for spindle actin assembly. Notably, previous studies have reported that the levels of Bub1 on kinetochore in human oocytes are rapidly downregulated at the onset of anaphase, with a similar temporal distribution observed in mouse (Yin et al., 2006; Lagirand-Cantaloube et al., 2017). In contrast, OsBRK1 has been shown to be a stable component of the kinetochore-associated proteins during meiosis in rice (Wang et al., 2012). In terms of molecular composition, OsBRK1 lacks the conserved GLEBS motifs and KEN box, which distinguishing it from its mammalian counterparts like Bub1 (Wang et al., 2012). Nonetheless, these data suggest that the role and regulation of Bub1 in meiosis might have diverged among different species. However, the kinase domain of OsBRK1 is quite conserved, indicating that OsBRK1 and its homologs are likely to perform similar cellular functions, including spindle actin assembly. Together, our findings bring a step-forward in advancing our knowledge of the assembly and regulation mechanism of meiotic spindle actin and reveal a function of kinetochore-localized proteins in the

regulation of spindle actin assembly, which also have important implications in spindle morphogenesis in various eukaryotes.

Materials and methods

Plant materials

The knockout plants of *OsBRK1*, *OsPFN2* and *OsPFN2*/*OsBRK1*(*Osbrk1*, *Ospfn2* and *Ospfn2-1Osbrk1* mutants) used in this study was generated in the *Oryza sativa subsp. japonica* cv. Nipponbare background. The *OsRMD* knockout plants used in this study is in *Oryza sativa subsp. japonica* cv. Kitaake background. The background of various transgenic plants (*OsPFN2:gOsPFN2*^{WT}, *OsPFN2:gOsPFN2*^{T21A}, *OsPFN2:gOsPFN2*^{T97A}, *OsPFN2:gOsPFN2*^{S100A}) were generated in the *Ospfn2-1* mutant. All rice plants were grown in paddy field at Nanjing Agricultural University (Nanjing, China) and Chinese Academy of Agricultural Sciences (Beijing, China) for phenotypic analyses.

Plasmid construction

To generate various CRISPR/Cas9 constructs, a 20-bp sequence of *OsBRK1*, *OsPFN2* and *OsRMD* were synthesized and cloned into the pOs-Cas9 vector (Miao et al., 2013). *OsPFN2*/*OsBRK1* genome editing constructs was performed as described previously (He et al., 2019). The CRISPR/Cas9 constructs were introduced into *japonica* Nipponbare or Kitaake via *Agrobacterium*-mediated transformation. To uncover the consequence of phosphorylation of OsPFN2, a 6.4-kb WT and mutant *OsPFN2* genomic DNA fragments (containing the 3-kb promoter and 1-kb 3'UTR region) were cloned into the pCAMBIA2300 vector, which were then introduced into the callus of the *Ospfn2-1* mutant (CRISPR/Cas9 free) using *Agrobacterium*-mediated transformation. All primer sequences are listed in Supplemental Table 2.

Recombinant protein and antibody preparation

Generate recombinant OsRMD FH1FH2 protein were performed as described previously (Zhang et al., 2011). To generate recombinant OsPFN2 and OsBRK1

proteins, the coding sequences of the *OsPFN2* and *OsBRK1* were amplified by PCR, respectively. Subsequently, the coding sequences of WT and mutant *OsPFN2,* and *OsBRK1* were cloned into the pET-28a and pMAL-c2X vectors, respectively. All primer sequences are listed in Supplemental Table 2. The fusion plasmids were transformed into *Escherichia coli* (DE3 strain). Protein expression was induced by the addition of 0.5 mM isopropyl β-D-thiogalactopyranoside (IPTG) for overnight at 16℃. *E. coli* was collected by centrifugation at 8000 g, and the *E. coli* pellet was resuspended with the protein buffer (150 mM KCl, 0.2 mM DTT, 20 mM Tris-HCl, pH 7.5). The resuspended bacterial was sonicated (pulse on 3 seconds, pulse off 5 seconds; amplitude 25%) to clear, supernatant (contained recombinant protein) was collected by centrifugation at 8000 g. The recombinant protein was collected by magnetic beads (Beaver), and released from the beads using protein eluent at 4℃. The recombinant protein was dialyzed overnight against the dialyzing buffer (5 mM Tris, 50 mM KCl, 0.5 mM DTT, and 0.5 mM EDTA), flash-frozen in liquid nitrogen and stored at -80℃. Actin was purified from rabbit skeletal muscle acetone powder as described previously (Huang et al., 2003). A peptide (C-QYKPEEITGIMKDFDE) derived from OsPFN2 was synthesized and injected into rabbits to produce polyclonal antibody against OsPFN2.

Protein interaction assay

For the Y2H assay, the full-length coding sequences of *OsPFN2*, *OsBRK1* and *OsRMD* were amplified and cloned into the pGADT7 and pGBKT7 vectors, respectively. Plasmids were co-transformed into the AH109 yeast strain using the Yeastmaker Yeast Transformation System (Clontech, 630439). Yeast strains were spread onto SD/-Trp-Leu plates and incubated for 5 days at 30℃. The yeast clones were diluted and spotted on the media SD/-Trp-Leu, SD/-Leu-Trp-His and SD/-Leu-Trp-His-Ade, respectively. All primer sequences are listed in Supplemental Table 2.

The bimolecular fluorescence complementation assays were performed as previously described (Zhou et al., 2013). The coding sequences of *OsPFN2*, *OsBRK1* and *OsRMD* were amplified by PCR and cloned into the p2YN and p2YC vector, respectively. Then the plasmids were transformed into *Agrobacterium* strain EHA105. *Agrobacterium*

strain with plasmids were infiltrated into *N. benthamiana* leaves and grew for 2 days. Fluorescence signals was observed under a Leica TCS SP8 confocal laser scanning microscope equipped with a ×10 objective (0.40-numerical aperture). Images were captured using a Leica Application Suite X 3.0 software.

The split-luciferase complementation imaging assays were performed as previously described (Chen et al., 2008). Full length coding sequence of *OsRMD*, *OsPFN2*^{WT}, mutant *OsPFN2* were amplified and cloned into the pCAMBIA-LUC vectors to fuse with the C-terminal fragment of luciferase (cLUC) and N-terminal fragment of luciferase (nLUC), respectively. The plasmids were transformed into *Agrobacterium* strain EHA105. *Agrobacterium* strain with plasmids were infiltrated into *N. benthamiana* leaves and grew for 2 days. The *N. benthamiana* leaves were treated using 1 mM luciferin (Promega, E1601) for 2 minutes at room temperature. Luciferase activities were detected using an imaging apparatus (NightShade LB 985, Berthold). All primer sequences are listed in Supplemental Table 2.

To examine the protein interaction, a co-immunoprecipitation assays was performed as previously described (Hu et al., 2020). The coding sequence of *OsRMD-C* (The C-terminal fragment of OsRMD, contained truncated FH1 and entire FH2 domain ranging from 3292 to 4881) and *OsBRK1* were amplified and cloned into the pCAMBIA1305-flag vector. The coding sequence of *OsPFN2* was amplified and cloned into the pCAMBIA1305-GFP vector. All plasmids were transformed into *Agrobacterium* strain EHA105. *Agrobacterium* strain with plasmids were infiltrated into *N. benthamiana* leaves and grew for 3 days. *N. benthamiana* leaves were ground into powder in liquid nitrogen and transferred to a centrifuge tube. Subsequently, 2 mL NB1 extraction buffer (50 mM Tris-HCl, pH 8.0, 1 mM $MgCl_2$, 0.5 M sucrose, 10 mM EDTA, 5 mM DTT, 1 × proteinase inhibitor cocktail, 1 × phosphatase inhibitor cocktail) was added to the centrifuge tube and incubated for 30 minutes on ice. The supernatant was collected after centrifugation at 12,000 g, 4℃ for 20 minutes, which was then transfer the supernatant to new centrifuge tube. 20 μL supernatant was used for input samples and the remaining supernatant was treated with flag beads (MBL, M185-10) for 2 hours at 4℃. The flag beads were rinsed for three times using the NB1 extraction buffer, and boiled in SDS

463 loading buffer. Protein bands were detected by western blot with anti-GFP (MBL, 598-
464 7) and anti-flag (MBL, M185-7) antibodies, respectively.

465 The coding sequence of *OsPFN2*^{WT} and mutant version of *OsPFN2* was amplified
466 and cloned into the pCAMBIA1305-GFP vector. All plasmids were transformed into
467 *Agrobacterium* strain EHA105. *Agrobacterium* strain with plasmids were infiltrated
468 into *N. benthamiana* leaves and grew for 3 days. The protein extraction method was
469 referred to Co-IP assay. The purified protein OsRMD FH1FH2 was incubated with
470 different versions of OsPFN2 protein extraction for 2 hours, and then treated with GST
471 beads (Beaver). The GST beads were rinsed for three times using the PBS buffer, and
472 boiled in SDS loading buffer. Protein bands were detected by western blot with Anti-
473 GFP (MBL, 598-7) and anti-GST (MBL, PM013-7) antibodies, respectively.

474 **Phosphorylation assay**

475 *In vitro* phosphorylation assays were performed as described previously (Hu et al.,
476 2020). Briefly, 2 μg OsBRK1-MBP and 1 μg OsPFN2-His were mixed in a
477 phosphorylation buffer (40 mM Hepes, pH 7.5, 20 mM $MgCl_2$, 2 mM DTT, 1 μCi [^{32}P]
478 γATP, 1 × proteinase inhibitor cocktail, 1 × phosphatase inhibitor cocktail) and
479 incubated for 30 minutes at 30℃, followed by the addition of SDS loading buffer. The
480 mixture was boiled for 10 minutes at 95℃ and the phosphorylation bands were
481 separated using 12.5% SDS-PAGE gels. The phosphorylation bands were exposed
482 using GE Amersham hyperfilm MP film.

483 **Observation of spindle actin and spindle microtubule**

484 To observe F-actin in meiotic pollen, fresh young panicles of rice were fixed with 4%
485 (w/v) paraformaldehyde in the PEM buffer (50 mM PIPES, 5 mM EGTA, 5 mM $MgSO_4$,
486 0.1 M mannitol, pH 6.9) at least 1 hour at room temperature. The meiotic anthers were
487 rinsed for three times using the PEM buffer. Afterwards, anthers were flattened on poly-
488 L-lysine-coated slides and pollens were released using tweezers. Slides were dried at
489 room temperature, and a thin layer 3% low melting agarose (Sigma, A2576) in the PEM
490 buffer was spread out on slides. The agarose blocks were soaked in the actin

fluorescence buffer (PEM buffer, 1.5% glycerol, 0.1% Triton X-100, 0.66 μM Alexa Fluor 488-phalloidin) for 6 hours. Chromosomes was stained with DAPI (diluted 1:1000 in the PEM buffer) for 30 minutes and then the agarose blocks were rinsed for three times using the PEM buffer. Spindle actin was observed with a Zeiss LSM980 confocal laser scanning microscope equipped with a ×63 oil objective (1.40-numerical aperture). Images were captured using a Zen 3.3 software. 3D images were obtained from confocal z-stacks with single images taken at the Z-step of 0.3 μm.

To observe spindle actin and spindle microtubule in meiotic pollen, fresh young panicles of rice were fixed with 4% (w/v) paraformaldehyde in the PHEMS buffer (60 mM PIPES, 25 mM HEPES, 10 mM EGTA, 2 mM $MgCl_2$, and 0.32 M sorbitol, pH 6.8) for at least 1 hour at room temperature. Meiotic anthers were rinsed using the PHEMS buffer, and pollens were released on poly-L-lysine-coated slides. Slides were dried at room temperature, and a thin layer 3% low melting agarose in the PHEMS buffer was spread out on the slides. The agarose blocks were soaked in 1.5% β-glucuronidase (Sigma, G-0751) in the PHEMS buffer overnight at room temperature and were rinsed for three times using the PBS buffer (0.14 M NaCl, 2.7 mM KCl, 10 mM Na_2HPO_4, and 1.8 mM KH_2PO_4, pH 7.2). Subsequently, the agarose blocks were incubated with mouse monoclonal anti-α-tubulin antibody (Sigma, T-9026; diluted 1:200 in PHEMS buffer) for 2 hours at room temperature. After wishing for three times with PBS, the agarose blocks were incubated with Alexa Fluor 488 goat anti-mouse antibody (Invitrogen, A11001; diluted 1:500 in PHEMS buffer) for 2 hours and 0.66 μM rhodamine phalloidin (Invitrogen, R415; diluted in PHEMS buffer) for 6 hours. The agarose blocks were incubated with DAPI (diluted 1:1000 in PHEMS buffer) for 30 minutes after washing with PBS for three times. Spindle actin and spindle microtubule were observed with a Zeiss LSM980 confocal laser scanning microscope equipped with a ×63 oil objective (1.40-numerical aperture). Images were captured using a Zen 3.3 software.

DAPI staining

For detection of chromosomes behavior, the young panicles of rice were fixed with

Carnoy's solution (ethanol:acetic=3:1) and stored at 4℃. The developmental stages of single anthers were estimated by acetate magenta staining. The remaining five anthers were squashed on poly-L-lysine-coated slides using 45% acetic acid, and pollens were released. The slides were flash-frozen in liquid nitrogen, and cover slips were removed subsequently. Chromosomes were stained with DAPI (diluted 1:1000 in PBS buffer) for 0.5 hour. Chromosomes were observed using fluorescence microscope (Leica DM5000B) equipped with a ×100 oil objective (1.40-numerical aperture). Images were captured using a Leica Application Suite 3.3.

Actin nucleation assay

Actin nucleation assay was performed as described previously (Huang et al., 2003; Liu et al., 2015). Briefly, actin (10% pyrene-labeled) was incubated with 200 nM OsRMD FH1FH2 and 3 μM OsPFN2 for 5 minutes at room temperature, and actin polymerization was initiated by the addition of one-tenth volume of the 10 × KMEI buffer (500 mM KCl, 10 mM $MgCl_2$, 10 mM EGTA, and 100 mM imidazole-HCl, pH 7.0). Pyrene fluorescence was monitored with a QuantaMaster Luminescence QM 3 PH Fluorometer (Photon Technology International) to trace actin polymerization.

Observation of embryo sac

Observation of embryo sac was performed as described previously (Zhao et al., 2013). The fresh mature panicles of rice were fixed with Carnoy's solution (ethanol:acetic=3:1) and incubated for 24 hours at room temperature. Embryo sacs were released using tweezers and pre-treated in 70% ethanol for 24 hours at room temperature. The embryo sacs were processed through an ethanol series (50%, 30% and 15%) with 2 hours for each step, and then transferred into distilled water. The embryo sacs were stained using 1% eosin-Y overnight at room temperature. All embryo sacs were rinsed for three times using distilled water and processed through an ethanol series (30%, 50%, 70%, 90%, and 100%). Finally, the embryo sacs were soaked in 1:1 ethanol and methyl salicylate for 1 hour, and cleared in methyl salicylate for 10 hours at room temperature. The embryo sacs were examined using a Zeiss LSM980 laser scanning microscopy

equipped with a ×10 objective (0.4-numerical aperture). Images were captured using a Zen 3.3 software.

Subcellular localization

Full length coding sequences of *OsRMD* were amplified by PCR and cloned into the pCAMBIA1305-GFP vector. Then the plasmids were transformed into *Agrobacterium* strain EHA105. *Agrobacterium* strain with plasmids were infiltrated into *N. benthamiana* leaves and grew for 2 days. Fluorescence signals was observed under Zeiss LSM980 laser scanning microscopy equipped with a ×10 objective (0.4-numerical aperture). Images were captured using a Zen 3.3 software.

β-Glucuronidase (GUS) histochemical staining

To detect the gene expression level of *OsPFN2*, a 2.7-kb promoter of *OsPFN2* was amplified by PCR and cloned into the pCAMBIA1381Z vector containing the *GUS* reporter gene. The plasmid was introduced into *japonica* Nipponbare by *Agrobacterium*-mediated transformation. Sample from the T_1 generation transgenic plants were soaked in the GUS staining solution as described previously (Bai et al., 2019). Then the samples were decolorized in 70% ethanol and images were captured by a stereomicroscope.

Total RNA extraction and qRT-PCR

Total RNA was extracted from various tissue of WT according to an RNA Prep Pure Plant kit manufacturer's manual (Tiangen, DP441). 2 μg of total RNA was reverse-transcribed using an oligo-dT or random primer and PrimeScript I (Takara). qRT-PCR was performed using a SYBR Premix Ex Taq kit (Takara) with an ABI prism 7500 Real Time PCR System (Thermo Fisher Scientific). The $2^{-\Delta\Delta CT}$ method was used to calculate relative changes in gene expression (Livak and Schmittgen, 2001). All primer sequences are listed in Supplemental Table 2.

Accession Numbers

Sequence from this study can be downloaded from the rice genome annotation project

(https://rice.uga.edu/) with the following accession numbers: *OsPFN1.1*, *LOC_Os10g17660*; *OsPFN1.2*, *LOC_Os10g17680*; *OsPFN2*, *LOC_Os6g05880*; *OsBRK1*, *LOC_Os07g32480*; *OsRMD*, *LOC_Os07g40510*; *OsGPAT6*, *LOC_Os10g27330*.

Author contributions

J.W., Z.G. and S.Z. supervised the project; H.Z., Z.G., S.Z. and S.H. designed the research; H.Z., C.W., H.W. and S.H. wrote the paper; H.Z. performed most of experiments; Y.R., J.S., X.Y., C.W., Z.X., B.Y., S.C., Y.H., S.Z., Q.W., J.L., Z.X., D.L., A.J., M.C., K.C., S.L., X.L., Y.T., L.J., Z.C., C.L., Q.L., X.G. and X.W. provided technical assistance.

Acknowledgements

This research was supported by the National Key Research and Development Program of China (2022YFD1201504, 2022YFF1002900), Innovation Program of Chinese Academy of Agricultural Sciences, and International Science & Technology Innovation Program of Chinese Academy of Agricultural Sciences (ASTIP), Biological Breeding-National Science and Technology Major Project (2023ZD040710510) and the China Postdoctoral Science Foundation (2022M723459).

Declaration of interests

The authors declare no competing interests.

Figure Legends

Figure 1. Spindle actin co-organizes with spindle microtubule in rice PMCs.

(A) Confocal images of spindle actin and spindle microtubules in WT rice PMCs. ImageJ software was used to measure the fluorescence intensity profile along the white lines. Spindle actin was detected with rhodamine phalloidin, spindle microtubules were detected with anti-α-tubulin antibody, and chromosomes were detected with DAPI (4',6-diamidino-2-phenylindole dihydrochloride). Scale bars, 5 μm.

(B) Schematic illustration of spindle actin and spindle microtubules in rice PMCs of

different stages during meiosis I as shown in (**A**).

(C) Schematic diagram showing the spatial association of spindle actin and spindle microtubule in WT rice PMCs.

Figure 2. Phenotypic characterization of WT and *Ospfn2* mutants.

(A) Creation of *Ospfn2* mutants using the CRISPR/Cas9 technology. Blank boxes, green boxes and black lines represent UTRs, exons and introns, respectively. The lower panel shows alignment of WT and *Ospfn2* mutant sequences at the CRISPR-Cas9 target sites. Red letter and dashed lines represent insertion or deletion (3-bp deletion in *Ospfn2-1*, 3-bp deletion and 1-bp insertion in *Ospfn2-2*).

(B) Amino acid sequence alignment of between $OsPFN2^{WT}$ and $OsPFN2^{-M}$ (refers to the one Methionine deletion of OsPFN2 in *Ospfn2-1* mutant). Red dashed box indicates mutation site.

(C) Pollen fertility of WT, *Ospfn2-1* and *Ospfn2-2* mutants. Dark-stained pollen is fertile and un-stained pollen is sterile. Scale bars, 100 μm.

(D) Detailed observation of *Ospfn2-1*. From left to right: adult plant, stained pollen and embryo sac of WT and *Ospfn2-1*. Dark-stained pollen is fertile and un-stained pollen is sterile. Scale bars, 20 cm (plant morphology), 100 μm (pollen staining), 50 μm (embryo sac).

(E) Plant height of WT and *Ospfn2-1*. Data are shown as mean ± SD, $n = 10$ adult plants.

(F) Quantification of pollen fertility of WT and *Ospfn2-1*. Data are shown as mean ± SD, $n = 3$ florets.

(G) *Ospfn2-1* had similar embryo sac fertility to WT. Data are shown as mean ± SD, $n = 3$ repeats.

(H) Chromosomes behavior in WT and *Ospfn2-1* mutant during meiosis. Chromosomes were detected with DAPI. Scale bars, 5 μm.

(I) Quantification of the frequency of PMCs with normal chromosomes behavior in WT and *Ospfn2-1* mutant. Data are shown as mean ± SD, $n = 3$ repeats.

Figure 3. Defective spindle actin assembly and spindle morphogenesis in *Ospfn2-1* mutant PMCs.

(A) Confocal images showing the organization of spindle actin and spindle microtubule in WT and *Ospfn2-1* mutant PMCs. Spindle actin was detected with rhodamine phalloidin, spindle microtubules were detected with anti-α-tubulin antibody, and chromosomes were detected with DAPI. Scale bars, 5 μm.

(B) Quantification of normalized fluorescence intensity of spindle actin in WT and *Ospfn2-1* mutant PMCs. Data are shown as mean ± SD, *n* = 23 PMCs for WT, 29 PMCs for *Ospfn2-1*, respectively.

(C) Categories for spindle morphology in WT and *Ospfn2-1* mutant. Red and green lines indicated spindle actin and spindle microtubule, respectively.

(D) Schematic depiction illustrating the length and width of spindle at metaphase I PMCs.

(E-G) Quantification of the length **(E)**, width **(F)** of spindle, and ratio of spindle length and width **(G)** in WT and the *Ospfn2-1* mutant PMCs at metaphase I. Data are shown as mean ± SD, *n* = 23 PMCs for WT, 29 PMCs for *Ospfn2-1* mutant, respectively.

Figure 4. Abnormal spindle formation and enhanced spindle actin filaments in the *Osbrk1* mutant PMCs.

(A) OsPFN2 protein is uniformly distributed in the cytoplasm of rice PMCs during meiosis I. OsPFN2 was detected with anti-OsPFN2 antibody, and chromosomes were stained with DAPI. Fluorescence intensity was scanned as indicated by white lines. Scale bars, 5 μm.

(B) Y2H assay showed that OsBRK1 physically interacts with OsPFN2. SD/-LT, Synthetic Dropout/-Leu-Trp; SD/-LTH, Synthetic Dropout/-Leu-Trp-His.

(C) BiFC assay showed that OsBRK1 physically interacts with OsPFN2 in the nucleus. D53-RFP were used as markers to indicate nucleus localization. Scale bars, 20 μm.

(D) Co-immunoprecipitation assay in *N. benthamiana* showed that OsBRK1 physically interacts with OsPFN2.

(E) Confocal images showing the organization of spindle actin and spindle

661 microtubules in PMCs of WT and the *Osbrk1* mutant. Spindle actin was detected with
662 rhodamine phalloidin, spindle microtubules were detected with anti-α-tubulin antibody,
663 and chromosomes were detected with DAPI. Scale bars, 5 μm.
664 **(F)** Quantification of normalized fluorescence intensity of spindle actin in WT and
665 *Osbrk1* mutant PMCs. Data are shown as mean ± SD, n = 25 PMCs for WT and *Osbrk1*,
666 respectively.
667 **(G-I)** Quantification of the length **(G)** and width **(H)** of spindle, and ratio of spindle
668 length and width **(I)** in the WT and *Osbrk1* mutant at metaphase I PMCs. Data are
669 shown as mean ± SD, n = 25 PMCs for WT and *Osbrk1*, respectively.
670
671 **Figure 5. OsBRK1-mediated phosphorylation of OsPFN2 is required for spindle**
672 **actin assembly and spindle morphogenesis.**
673 **(A)** OsBRK1 could phosphorylate OsPFN2 in autoradiography assay (upper panel) and
674 SDS-PAGE (lower panel).
675 **(B)** Replacement of Thr21 (OsPFN2^{T21}), Thr97 (OsPFN2^{T97}) and Ser100 (OsPFN2^{S100})
676 with alanine in OsPFN2 significantly reduced the phosphorylation level mediated by
677 OsBRK1, compared to that of OsPFN2^{WT}. In parallel, three other substitutions
678 (OsPFN2^{S36A}, OsPFN2^{T63A} and OsPFN2^{T70A}) were created as negative controls, as they
679 were not detected in LC-MS/MS analysis. Upper panel, autoradiography assay; lower
680 panel, SDS-PAGE.
681 **(C)** OsPFN2^{WT}, OsPFN2^{T21D}, OsPFN2^{T97D} and OsPFN2^{S100D} inhibit spontaneous actin
682 polymerization with similar capability.
683 **(D)** Diagram of the *OsPFN2:gOsPFN2*^{WT} and version of mutated *OsPFN2* construct.
684 p*OsPFN2*, promoter of *OsPFN2*.
685 **(E)** Pollen fertility and meiotic spindle actin of the *Ospfn2-1* plants transformed with
686 *OsPFN2:gOsPFN2*^{WT} and the phosphorylation-attenuated OsPFN2 mutant versions
687 (*OsPFN2:gOsPFN2*^{T21A}, *OsPFN2:gOsPFN2*^{T97A} and *OsPFN2:gOsPFN2*^{S100A}). Pollens
688 were stained with KI-I_2. Dark pollens were fertile and the un-stained pollens were
689 sterile. Spindle actin was stained with rhodamine phalloidin, and chromosomes were
690 stained with DAPI. Scale bars, 100 μm (upper panel) or 5 μm (lower panel).

(F) Expression of *OsPFN2* in *Ospfn2-1* plants transformed with *OsPFN2:gOsPFN2*^{WT} and the phosphorylation-attenuated OsPFN2 mutant versions (*OsPFN2:gOsPFN2*^{T21A}, *OsPFN2:gOsPFN2*^{T97A} and *OsPFN2:gOsPFN2*^{S100A}).

(G) Quantification of pollen fertility of WT, *Ospfn2-1* mutant, *OsPFN2:gOsPFN2*^{WT}*/Ospfn2-1*, *OsPFN2:gOsPFN2*^{T21A}*/Ospfn2-1*, *OsPFN2:gOsPFN2*^{T97A}*/Ospfn2-1* and *OsPFN2:gOsPFN2*^{S100A}*/Ospfn2-1* plants. Data are shown as mean ± SD, *n* = 3 florets.

(H) Quantification of normalized fluorescence intensity of spindle actin in the WT, *Ospfn2-1* mutant, *OsPFN2:gOsPFN2*^{WT}*/Ospfn2-1*, *OsPFN2:gOsPFN2*^{T21A}*/Ospfn2-1*, *OsPFN2:gOsPFN2*^{T97A}*/Ospfn2-1* and *OsPFN2:gOsPFN2*^{S100A}*/Ospfn2-1* PMCs. Data are shown as mean ± SD, *n* = 18, 26, 20, 22, 26, 18 PMCs.

(I-K) the length **(I)** and width **(J)** of spindle, and ratio of spindle length and width **(K)** in the WT, *Ospfn2-1* mutant, *OsPFN2:gOsPFN2*^{WT}*/Ospfn2-1*, *OsPFN2:gOsPFN2*^{T21A}*/Ospfn2-1*, *OsPFN2:gOsPFN2*^{T97A}*/Ospfn2-1* and *OsPFN2:gOsPFN2*^{S100A}*/Ospfn2-1* at metaphase I. Data are shown as mean ± SD, *n* = 18, 26, 20, 22, 26, 18 PMCs.

Figure 6. OsRMD fails to efficiently utilize phosphomimic actin-OsPFN2 complexes in forming a module for spindle actin assembly.

(A) Confocal images showing the organization of spindle actin and spindle microtubules in PMCs of WT and the *Osrmd* mutant. Spindle actin was detected with rhodamine phalloidin, spindle microtubules were detected with anti-α-tubulin antibody, and chromosomes were detected with DAPI. Scale bars, 5 μm.

(B) Quantification of normalized fluorescence intensity of spindle actin in WT and *Osrmd* mutant PMCs. Data are shown as mean ± SD, *n* = 21 PMCs for WT, 20 PMCs for *Osrmd* mutant, respectively.

(C-E) Quantification of the length **(C)**, width **(D)** of spindle, and ratio of spindle length and width **(E)** in the WT and *Osrmd* mutant PMCs at metaphase I. Data are shown as mean ± SD, *n* = 21 PMCs for WT, 20 PMCs for *Osrmd* mutant, respectively.

(F) Time course of OsRMD-mediated actin polymerization in the presence of $OsPFN2^{WT}$, or its phosphomimic versions, $OsPFN2^{T21D}$, $OsPFN2^{T97D}$, and $OsPFN2^{S100D}$.

(G) The interaction of OsRMD with the phospho-mimic forms of OsPFN2 was weaker than with $OsPFN2^{WT}$ as shown by semi-*vivo* protein interact assay.

(H) The interaction of OsRMD with the phospho-mimic forms of OsPFN2 was weaker than with $OsPFN2^{WT}$ as shown by firefly luciferase complementation assay using the leaf epidermal cells of *N. benthamiana*. cLUC, C terminus of LUC; nLUC, N terminus of LUC. OsGPAT6 was used as negative controls.

Figure 7. A proposed working model for the regulation of accurate formation of spindle actin.

OsPFN2 interact with OsRMD to form OsPFN2-OsRMD module that facilitates the assembly of spindle actin, ensure proper spindle morphogenesis. Disruption of function of the OsPFN2-OsRMD module result in abnormal assembly of spindle actin and spindle microtubule, which leads to incompact spindle morphology. In addition, OsPFN2 is constantly subjected to phosphorylation by OsBRK1 to maintain a homeostatic phosphorylation level. As OsPFN2 and phosphorylated OsPFN2 have similar capability in binding to actin monomers, actin monomers exist in the forms of either bound with OsPFN2 or phosphorylated OsPFN2. The ratio of actin monomers bound with OsPFN2 to actin monomers bound with phosphorylated OsPFN2 dictates the functionality of formin (e.g. OsRMD) in spindle actin polymerization, as formin has reduced capability in binding to and utilizing actin monomers bound with phosphorylated OsPFN2. As a result, OsBRK1-mediated phosphorylation of OsPFN2 to regulate function of OsPFN2-OsRMD module for the accurate formation of spindle actin in rice PMCs. Spindle actin filaments are maintained at a proper level, bound with spindle microtubules, ensure properly spindle morphogenesis during meiosis.

Supplemental Information

Supplemental Figure 1. Spindle actin in rice PMCs.

Supplemental Figure 2. Expression pattern of profilin genes in rice.

Supplemental Figure 3. The dysfunction of OsPFN2 leads to the delayed tapetum degradation and defective pollen exine formation.

Supplemental Figure 4. A proposed model showing that OsPFN2 promote the assembly of spindle actin.

Supplemental Figure 5. Creation of the *Osbrk1* and *Osrmd* mutant using the CRISPR/Cas9 technology.

Supplemental Figure 6. LC-MS/MS analysis revealed that Thr21 (A), Thr97 (B) and Ser100 (C) of OsPFN2 were phosphorylated by OsBRK1.

Supplemental Figure 7. OsBRK1 acts upstream of OsPFN2 to regulate spindle actin assembly.

Supplemental Figure 8. OsPFN2 interacts OsRMD with to form the OsPFN2-OsRMD module.

Supplemental Figure 9. Subcellular localization assay shows that co-expression of GFP-OsRMD, MAP65-RFP (microtubule marker) and FABD2-CFP (F-actin marker) in leaf epidermal cells of *N. benthamiana*.

Supplemental Figure 10. Subcellular localization assay shows that GFP-OsGPAT6 in leaf epidermal cells of *N. benthamiana* in support to split-luciferase complementation assay performed in this study.

Supplemental Figure 11. OsPFN2^{-M} retains the capability in inhibiting spontaneous actin assembly whereas actin-OsPFN2^{-M} has reduced activity in promoting actin assembly.

Supplemental Movie 1. 3D movie of spindle actin at diakinesis in a rice PMC. Spindle actin (phalloidin), chromosome (DAPI).

Supplemental Movie 2. 3D movie of spindle actin at metaphase I in a rice PMC. Spindle actin (phalloidin), chromosome (DAPI).

Supplemental Movie 3. 3D movie of spindle actin at anaphase I in a rice PMC. Spindle actin (phalloidin), chromosome (DAPI).

Supplemental Movie 4. 3D movie of spindle actin at telophase I in a rice PMC. Spindle actin (phalloidin), chromosome (DAPI).

779 **Supplemental Movie 5.** 3D movie of spindle actin at dyad in a rice PMC. Spindle actin
780 (phalloidin), chromosome (DAPI).
781 **Supplemental Table 1.** Screening in rice meiotic anther yeast library using OsPFN2 as
782 bait.
783 **Supplemental Table 2.** Primers used in this study.
784

References

Akera, T., Chmátal, L., Trimm, E., Yang, K., Aonbangkhen, C., Chenoweth, D.M., Janke, C., Schultz, R.M., and Lampson, M.A. (2017). Spindle asymmetry drives non-Mendelian chromosome segregation. Science **358**:668-672. 10.1126/science.aan0092.

Bai, W., Wang, P., Hong, J., Kong, W., Xiao, Y., Yu, X., Zheng, H., You, S., Lu, J., Lei, D., et al. (2019). *Earlier Degraded Tapetum1* (*EDT1*) encodes an ATP-Citrate Lyase required for tapetum programmed cell death. Plant Physiol **181**:1223-1238. 10.1104/pp.19.00202.

Bernard, P., Maure, J.F., and Javerzat, J.P. (2001). Fission yeast Bub1 is essential in setting up the meiotic pattern of chromosome segregation. Nat Cell Biol **3**:522-526. 10.1038/35074598.

Cao, L.Y., Henty-Ridilla, J.L., Blanchoin, L., and Staiger, C.J. (2016). Profilin-dependent nucleation and assembly of actin filaments controls cell elongation in *Arabidopsis*. Plant Physiol **170**:220-233. 10.1104/pp.15.01321.

Chen, C., Marcus, A., Li, W., Hu, Y., Calzada, J.P.V., Grossniklaus, U., Cyr, R.J., and Ma, H. (2002). The *Arabidopsis ATK1* gene is required for spindle morphogenesis in male meiosis. Development **129**:2401-2409. 10.1242/dev.129.10.2401.

Chen, H., Zou, Y., Shang, Y., Lin, H., Wang, Y., Cai, R., Tang, X., and Zhou, J. (2008). Firefly luciferase complementation imaging assay for protein-protein interactions in plants. Plant Physiol **146**:368-376. 10.1104/pp.107.111740.

Courtemanche, N. (2018). Mechanisms of formin-mediated actin assembly and dynamics. Biophys Rev **10**:1553-1569. 10.1007/s12551-018-0468-6.

Deng, X.G., Peng, F., Tang, X., Lee, Y.R.J., Lin, H., and Liu, B. (2024). The *Arabidopsis* BUB1/MAD3 family protein BMF3 requires BUB3.3 to recruit CDC20 to kinetochores in spindle assembly checkpoint signaling. Proc Natl Acad Sci U S A **121**:e2322677121. 10.1073/pnas.2322677121.

Dunkley, S., and Mogessie, B. (2023). Actin limits egg aneuploidies associated with female reproductive aging. Sci Adv **9**:eadc9161. 10.1126/sciadv.adc9161.

He, Y., Wang, C., Higgins, J.D., Yu, J., Zong, J., Lu, P., Zhang, D., and Liang, W. (2016). Meiotic F-box is essential for male meiotic DNA double-strand break repair in rice. Plant Cell **28**:1879-1893. 10.1105/tpc.16.00108.

He, Y., Zhu, M., Wang, L., Wu, J., Wang, Q., Wang, R., and Zhao, Y. (2019). Improvements of TKC technology accelerate isolation of Transgene-Free CRISPR/Cas9-Edited rice plants. Rice Sci **26**:109-117. 10.1016/j.rsci.2018.11.001.

Henty-Ridilla, J.L., Juanes, M.A., and Goode, B.L. (2017). Profilin directly promotes microtubule growth through residues mutated in amyotrophic lateral sclerosis. Curr Biol **27**:3535-3543. 10.1016/j.cub.2017.10.002.

Holubcová, Z., Blayney, M., Elder, K., and Schuh, M. (2015). Error-prone chromosome-mediated spindle assembly favors chromosome segregation defects in human oocytes. Science **348**:1143-1147. 10.1126/science.aaa9529.

Hu, J., Huang, J., Xu, H., Wang, Y., Li, C., Wen, P., You, X., Zhang, X., Pan, G., Li, Q., et al. (2020). Rice stripe virus suppresses jasmonic acid-mediated resistance by hijacking brassinosteroid signaling pathway in rice. PLoS Pathog **16**:e1008801. 10.1371/journal.ppat.1008801.

Huang, S., Blanchoin, L., Kovar, D.R., and Staiger, C.J. (2003). *Arabidopsis* capping protein (AtCP) is a heterodimer that regulates assembly at the barbed ends of actin filaments. J Biol Chem **278**:44832-44842. 10.1074/jbc.M306670200.

Ji, Z., Gao, H., and Yu, H. (2015). Kinetochore attachment sensed by competitive Mps1 and microtubule binding to Ndc80C. Science **348**:1260-1264. 10.1126/science.aaa4029.

Jiang, H., Wang, F., Wu, Y., Zhou, X., Huang, X., Zhu, J., Gao, J., Dong, R., Cao, K., and Yang, Z. (2009). MULTIPOLAR SPINDLE 1 (MPS1), a novel coiled-coil protein of *Arabidopsis thaliana*, is required for meiotic spindle organization. Plant J **59**:1001-1010. 10.1111/j.1365-313X.2009.03929.x.

Kawashima, S.A., Yamagishi, Y., Honda, T., Ishiguro, K., and Watanabe, Y. (2010). Phosphorylation of H2A by Bub1 prevents chromosomal instability through localizing Shugoshin. Science **327**:172-177. 10.1126/science.1180189.

Kim, S.J., Sun, H.B., Tomchick, D.R., Yu, H., and Luo, X. (2012). Structure of

human Mad1 C-terminal domain reveals its involvement in kinetochore targeting. Proc Natl Acad Sci U S A **109**:6549-6554. 10.1073/pnas.1118210109.

Kitajima, T.S., Kawashima, S.A., and Watanabe, Y. (2004). The conserved kinetochore protein shugoshin protects centromeric cohesion during meiosis. Nature **427**:510-517. 10.1038/nature02312.

Klebig, C., Korinth, D., and Meraldi, P. (2009). Bub1 regulates chromosome segregation in a kinetochore-independent manner. J Cell Biol **185**:841-858. 10.1083/jcb.200902128.

Komaki, S., and Schnittger, A. (2016). The spindle checkpoint in plants - a green variation over a conserved theme? Curr Opin Plant Biol **34**:84-91. 10.1016/j.pbi.2016.10.008.

Kovar, D.R. (2006). Molecular details of formin-mediated actin assembly. Curr Opin Cell Biol **18**:11-17. 10.1016/j.ceb.2005.12.011.

Lagirand-Cantaloube, J., Ciabrini, C., Charrasse, S., Ferrieres, A., Castro, A., Anahory, T., and Lorca, T. (2017). Loss of centromere cohesion in aneuploid human oocytes correlates with decreased kinetochore localization of the Sac proteins Bub1 and Bubr1. Sci Rep **7**:44001. 10.1038/srep44001.

Lampson, M.A., and Cheeseman, I.M. (2011). Sensing centromere tension: Aurora B and the regulation of kinetochore function. Trends Cell Biol **21**:133-140. 10.1016/j.tcb.2010.10.007.

Lee, Y.R.J., and Liu, B. (2019). Microtubule nucleation for the assembly of acentrosomal microtubule arrays in plant cells. New Phytol **222**:1705-1718. 10.1111/nph.15705.

Lee, Y.R.J., Qiu, W., and Liu, B. (2015). Kinesin motors in plants: from subcellular dynamics to motility regulation. Curr Opin Plant Biol **28**:120-126. 10.1016/j.pbi.2015.10.003.

Li, G., Yang, X., Zhang, X., Song, Y., Liang, W., and Zhang, D. (2018). Rice morphology determinant-mediated actin filament organization contributes to pollen tube growth. Plant Physiol **177**:255-270. 10.1104/pp.17.01759.

Li, Y., Shen, Y., Cai, C., Zhong, C., Zhu, L., Yuan, M., and Ren, H. (2010). The

type II *Arabidopsis* formin14 interacts with microtubules and microfilaments to regulate cell division. Plant Cell **22**:2710-2726. 10.1105/tpc.110.075507.

Liu, B., and Lee, Y.J. (2022). Spindle assembly and mitosis in plants. Annu Rev Plant Biol **73**:227-254. 10.1146/annurev-arplant-070721-084258.

Liu, B., Ho, C.M.K., and Lee, Y.R.J. (2011). Microtubule reorganization during mitosis and cytokinesis: lessons learned from developing microgametophytes in *Arabidopsis Thaliana*. Front Plant Sci **2**:27. 10.3389/fpls.2011.00027.

Liu, C., Zhang, Y., and Ren, H. (2021). Profilin promotes formin-mediated actin filament assembly and vesicle transport during polarity formation in pollen. Plant Cell **33**:1252-1267. 10.1093/plcell/koab027.

Liu, X., Qu, X., Jiang, Y., Chang, M., Zhang, R., Wu, Y., Fu, Y., and Huang, S. (2015). Profilin regulates apical actin polymerization to control polarized pollen tube growth. Mol Plant **8**:1694-1709. 10.1016/j.molp.2015.09.013.

Livak, K.J., and Schmittgen, T.D. (2001). Analysis of relative gene expression data using real-time quantitative PCR and the $2^{-\Delta\Delta CT}$ Method. Methods **25**:402-408. 10.1006/meth.2001.1262.

London, N., and Biggins, S. (2014). Mad1 kinetochore recruitment by Mps1-mediated phosphorylation of Bub1 signals the spindle checkpoint. Genes Dev **28**:140-152. 10.1101/gad.233700.113.

Lv, G., Li, Y., Wu, Z., Zhang, Y., Li, X., Wang, T., Ren, W., Liu, L., Chen, J., and Zhang, Y. (2024). Maize *actin depolymerizing factor 1* (*ZmADF1*) negatively regulates pollen development. Biochem Biophys Res Commun **703**:149637. 10.1016/j.bbrc.2024.149637.

McAinsh, A.D., and Kops, G.J.P.L. (2023). Principles and dynamics of spindle assembly checkpoint signalling. Nat Rev Mol Cell Biol **24**:543-559. 10.1038/s41580-023-00593-z.

McMichael, C.M., and Bednarek, S.Y. (2013). Cytoskeletal and membrane dynamics during higher plant cytokinesis. New Phytol **197**:1039-1057. 10.1111/nph.12122.

Mercier, R., Mezard, C., Jenczewski, E., Macaisne, N., and Grelon, M. (2015). The molecular biology of meiosis in plants. Annu Rev Plant Biol **66**:297-327.

10.1146/annurev-arplant-050213-035923.

Miao, J., Guo, D., Zhang, J., Huang, Q., Qin, G., Zhang, X., Wan, J., Gu, H., and Qu, L.J. (2013). Targeted mutagenesis in rice using CRISPR-Cas system. Cell Res **23**:1233-1236. 10.1038/cr.2013.123.

Mogessie, B., and Schuh, M. (2017). Actin protects mammalian eggs against chromosome segregation errors. Science **357**:eaal1647. 10.1126/science.aal1647.

Musacchio, A. (2015). The molecular biology of spindle assembly checkpoint signaling dynamics. Curr Biol **25**:R1002-R1018. 10.1016/j.cub.2015.08.051.

Musacchio, A., and Salmon, E.D. (2007). The spindle-assembly checkpoint in space and time. Nat Rev Mol Cell Biol **8**:379-393. 10.1038/nrm2163.

Roeles, J., and Tsiavaliaris, G. (2019). Actin-microtubule interplay coordinates spindle assembly in human oocytes. Nat Commun **10**:4651. 10.1038/s41467-019-12674-9.

Sacristan, C., and Kops, G.J.P.L. (2015). Joined at the hip: kinetochores, microtubules, and spindle assembly checkpoint signaling. Trends Cell Biol **25**:21-28. 10.1016/j.tcb.2014.08.006.

Schuh, M., and Ellenberg, J. (2008). A new model for asymmetric spindle positioning in mouse oocytes. Curr Biol **18**:1986-1992. 10.1016/j.cub.2008.11.022.

Sheykhani, R., Baker, N., Gomez-Godinez, V., Liaw, L.H., Shah, J., Berns, M.W., and Forer, A. (2013). The role of actin and myosin in PtK2 spindle length changes induced by laser microbeam irradiations across the spindle. Cytoskeleton **70**:241-259. 10.1002/cm.21104.

Shi, W., Ji, J., Xue, Z., Zhang, F., Miao, Y., Yang, H., Tang, D., Du, G., Li, Y., Shen, Y., et al. (2021). PRD1, a homologous recombination initiation factor, is involved in spindle assembly in rice meiosis. New Phytol **230**:585-600. 10.1111/nph.17178.

Staiger, C.J.C., and Cande, Z. (1991). Microfilament distribution in maize meiotic mutants correlates with microtubule organization. Plant Cell **3**:637-644. 10.1105/tpc.3.6.637.

Sun, T., Li, S., and Ren, H. (2013). Profilin as a regulator of the membrane-actin cytoskeleton interface in plant cells. Front Plant Sci **4**:512.

10.3389/fpls.2013.00512.

Sun, H., Qiao, Z., Chua, K.P., Tursic, A., Liu, X., Gao, Y.G., Mu, Y., Hou, X., and Miao, Y. (2018). Profilin negatively regulates formin-mediated actin assembly to modulate PAMP-triggered plant immunity. Curr Biol **28**:1882-1895. 10.1016/j.cub.2018.04.045.

Touati, S.A., and Wassmann, K. (2016). How oocytes try to get it right: spindle checkpoint control in meiosis. Chromosoma **125**:321-335. 10.1007/s00412-015-0536-7.

Ullrich, C.I., Aloni, R., Saeed, M.E.M., Ullrich, W., and Efferth, T. (2019). Comparison between tumors in plants and human beings: Mechanisms of tumor development and therapy with secondary plant metabolites. Phytomedicine **64**:153081. 10.1016/j.phymed.2019.153081.

Vleugel, M., Hoek, T.A., Tromer, E., Sliedrecht, T., Groenewold, V., Omerzu, M., and Kops, G.J.P.L. (2015). Dissecting the roles of human BUB1 in the spindle assembly checkpoint. J Cell Sci **128**:2975-2982. 10.1242/jcs.169821.

Wang, M., Tang, D., Luo, Q., Jin, Y., Shen, Y., Wang, K., and Cheng, Z. (2012). BRK1, a Bub1-related kinase, is essential for generating proper tension between homologous kinetochores at metaphase I of rice meiosis. Plant Cell **24**:4961-4973. 10.1105/tpc.112.105874.

Wood, B.W., Shi, X.Z., and Weil, T.T. (2024). F-actin coordinates spindle morphology and function in meiosis. PLoS Genet **20**:e1011111. 10.1371/journal.pgen.1011111.

Xu, C., Liu, Z., Zhang, L., Zhao, C., Yuan, S., and Zhang, F. (2013). Organization of actin cytoskeleton during meiosis I in a wheat thermo-sensitive genic male sterile line. Protoplasma **250**:415-422. 10.1007/s00709-012-0386-6.

Xue, Z., Liu, C., Shi, W., Miao, Y., Shen, Y., Tang, D., Li, Y., You, A., Xu, Y., Chong, K., et al. (2019). OsMTOPVIB is required for meiotic bipolar spindle assembly. Proc Natl Acad Sci U S A **116**:15967-15972. 10.1073/pnas.1821315116.

Yang, W., Ren, S., Zhang, X., Gao, M., Ye, S., Qi, Y., Zheng, Y., Wang, J., Zeng, L., Li, Q., et al. (2011). *BENT UPPERMOST INTERNODE1* encodes the class II formin FH5 crucial for actin organization and rice development. Plant Cell **23**:661-

680. 10.1105/tpc.110.081802.

Ye, J., and Xu, M. (2012). Actin bundler PLIM2s are involved in the regulation of pollen development and tube growth in *Arabidopsis*. J Plant Physiol **169**:516-522. 10.1016/j.jplph.2011.11.015.

Yin, S., Wang, Q., Liu, J., Ai, J., Liang, C., Hou, Y., Chen, D., Schatten, H., and Sun, Q. (2006). Bub1 prevents chromosome misalignment and precocious anaphase during mouse oocyte meiosis. Cell Cycle **5**:2130-2137. 10.4161/cc.5.18.3170.

Zhang, D., Luo, X., and Zhu, L. (2011). Cytological analysis and genetic control of rice anther development. J Genet Genomics **38**:379-390. 10.1016/j.jgg.2011.08.001.

Zhang, H., Deng, X.G., Sun, B., Van, S.L., Kang, Z., Lin, H., Lee, Y.R.J., and Liu, B. (2018). Role of the BUB3 protein in phragmoplast microtubule reorganization during cytokinesis. Nat Plants **4**:485-494. 10.1038/s41477-018-0192-z.

Zhang, Z., Zhang, Y., Tan, H., Wang, Y., Li, G., Liang, W., Yuan, Z., Hu, J., Ren, H., and Zhang, D. (2011). *RICE MORPHOLOGY DETERMINANT* encodes the type II formin FH5 and regulates rice morphogenesis. Plant Cell **23**:681-700. 10.1105/tpc.110.081349.

Zhang, Y., Dong, G., Wu, L., Wang, X., Chen, F., Xiong, E., Xiong, G., Zhou, Y., Kong, Z., Fu, Y., et al. (2023). Formin protein DRT1 affects gross morphology and chloroplast relocation in rice. Plant Physiol **191**:280-298. 10.1093/plphys/kiac427.

Zhao, Z., Zhang, Y., Liu, X., Zhang, X., Liu, S., Yu, X., Ren, Y., Zheng, X., Zhou, K., Jiang, L., et al. (2013). A role for a Dioxygenase in auxin metabolism and reproductive development in rice. Dev Cell **27**:113-122. 10.1016/j.devcel.2013.09.005.

Zhou, Y., Li, Y., You, H., Chen, J., Wang, B., Wen, M., Zhang, Y., Tang, D., Shen, Y., Yu, H., et al. (2024). Kinesin-1-like protein PSS1 is essential for full-length homologous pairing and synapsis in rice meiosis. Plant J **120**:928-940. 10.1111/tpj.17025.

995 **Zhou, S., Wang, Y., Li, W., Zhao, Z., Ren, Y., Wang, Y., Gu, S., Lin, Q., Wang, D.,**
996 **Jiang, L., et al.** (2011). *Pollen semi-sterility1* encodes a kinesin-1-like protein
997 important for male meiosis, anther dehiscence, and fertility in rice. Plant Cell
998 **23**:111-129. 10.1105/tpc.109.073692.
999 **Zhou, F., Lin, Q., Zhu, L., Ren, Y., Zhou, K., Shabek, N., Wu, F., Mao, H., Dong,**
1000 **W., Gan, L., et al.** (2013). D14-SCF$^{(D3)}$-dependent degradation of D53 regulates
1001 strigolactone signalling. Nature **504**:406-410. 10.1038/nature12878.

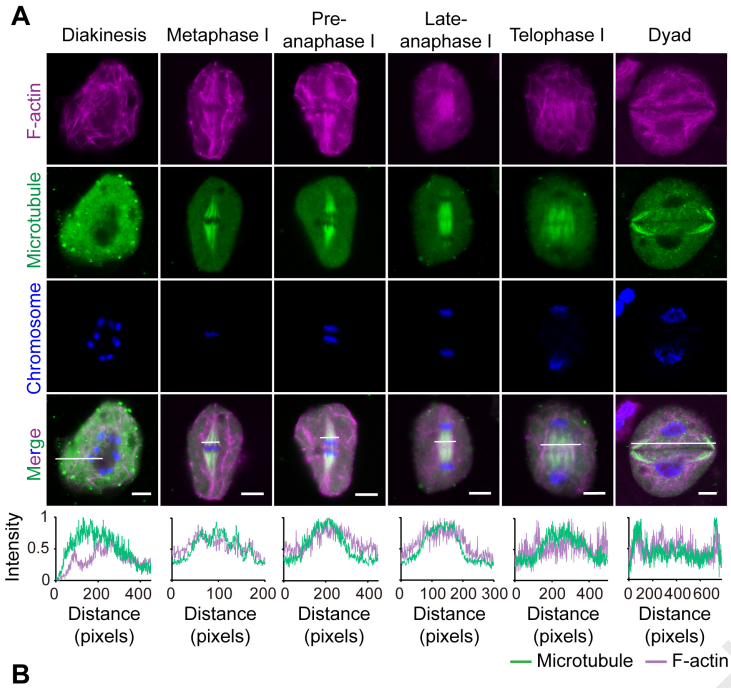

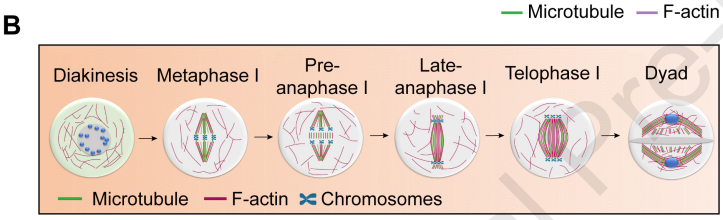

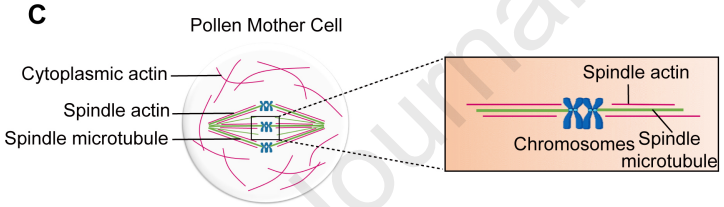

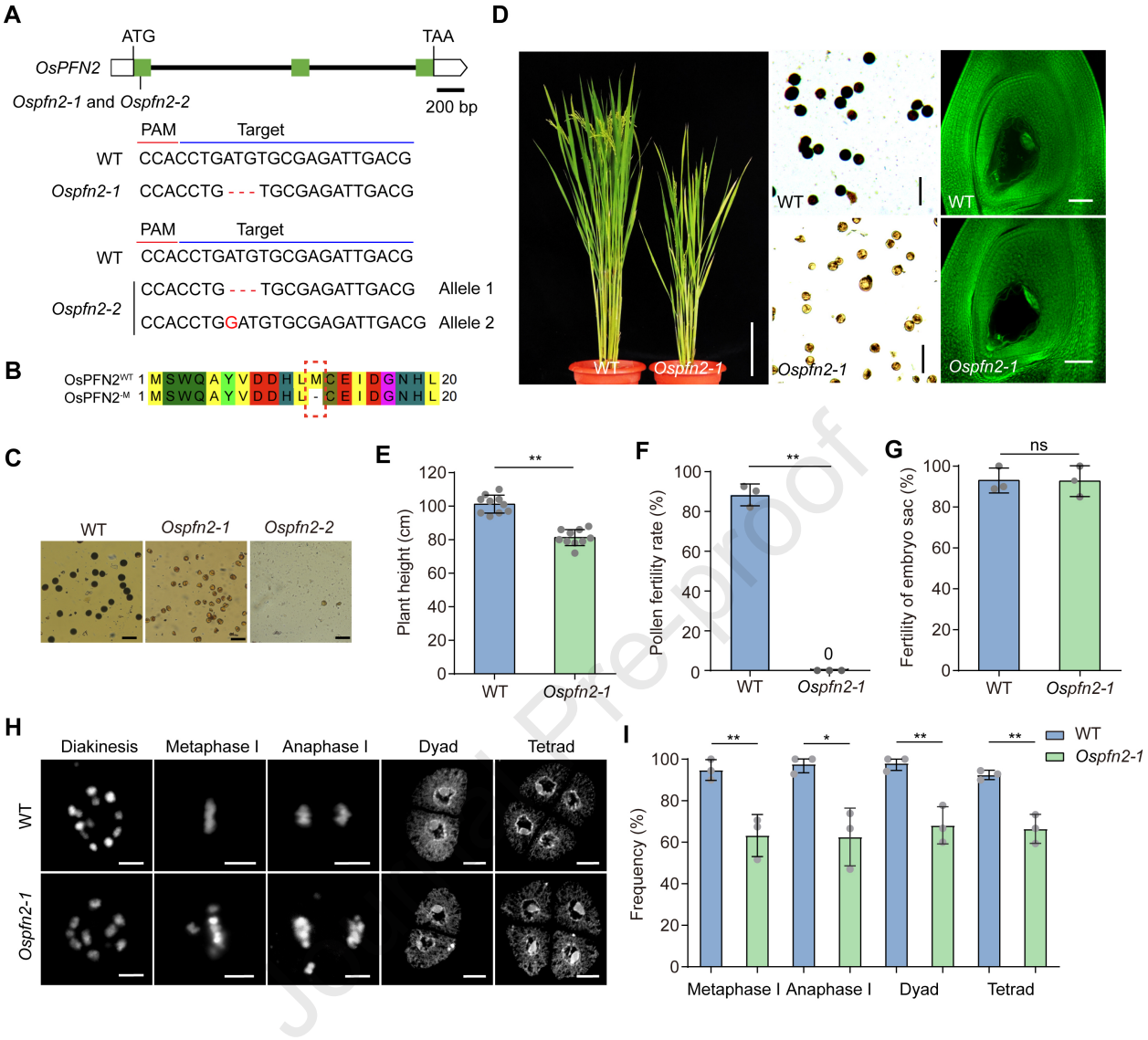
A
ATG
TAA
OsPFN2
Ospfn2-1 and Ospfn2-2
200 bp
PAM
Target
WT CCACCTGATGTGCGAGATTGACG
Ospfn2-1 CCACCTG - - - TGCGAGATTGACG
PAM
Target
WT CCACCTGATGTGCGAGATTGACG
Ospfn2-2 CCACCTG - - - TGCGAGATTGACG Allele 1
CCACCTGGATGTGCGAGATTGACG Allele 2
B
OsPFN2WT 1 M S W Q A Y V D D H L M C E I D G N H L 20
OsPFN2-M 1 M S W Q A Y V D D H L - C E I D G N H L 20
C
WT
Ospfn2-1
Ospfn2-2
D
WT
Ospfn2-1
E
Plant height (cm)
WT
Ospfn2-1
F
Pollen fertility rate (%)
WT
Ospfn2-1
G
Fertility of embryo sac (%)
ns
WT
Ospfn2-1
H
Diakinesis
Metaphase I
Anaphase I
Dyad
Tetrad
WT
Ospfn2-1
I
Frequency (%)
WT
Ospfn2-1
Metaphase I
Anaphase I
Dyad
Tetrad

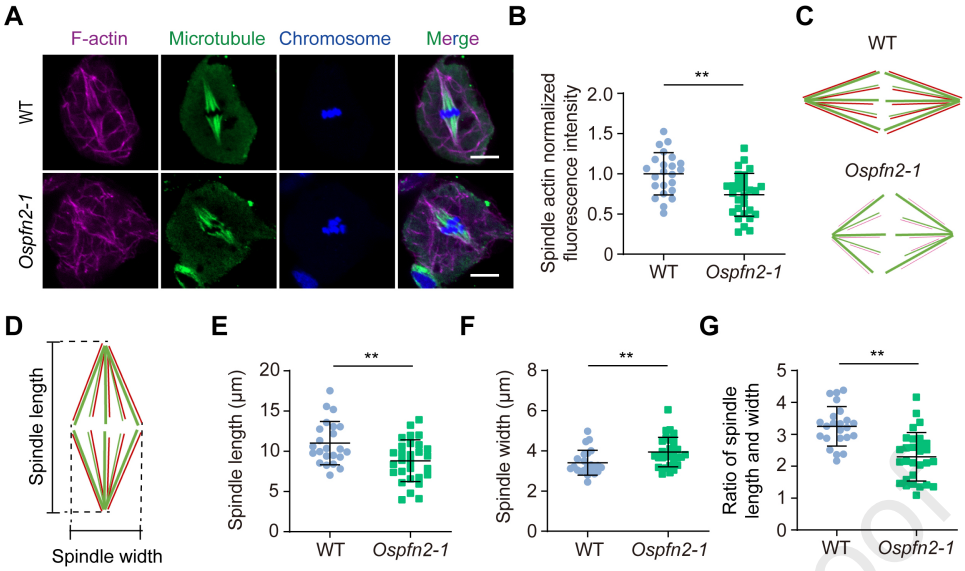

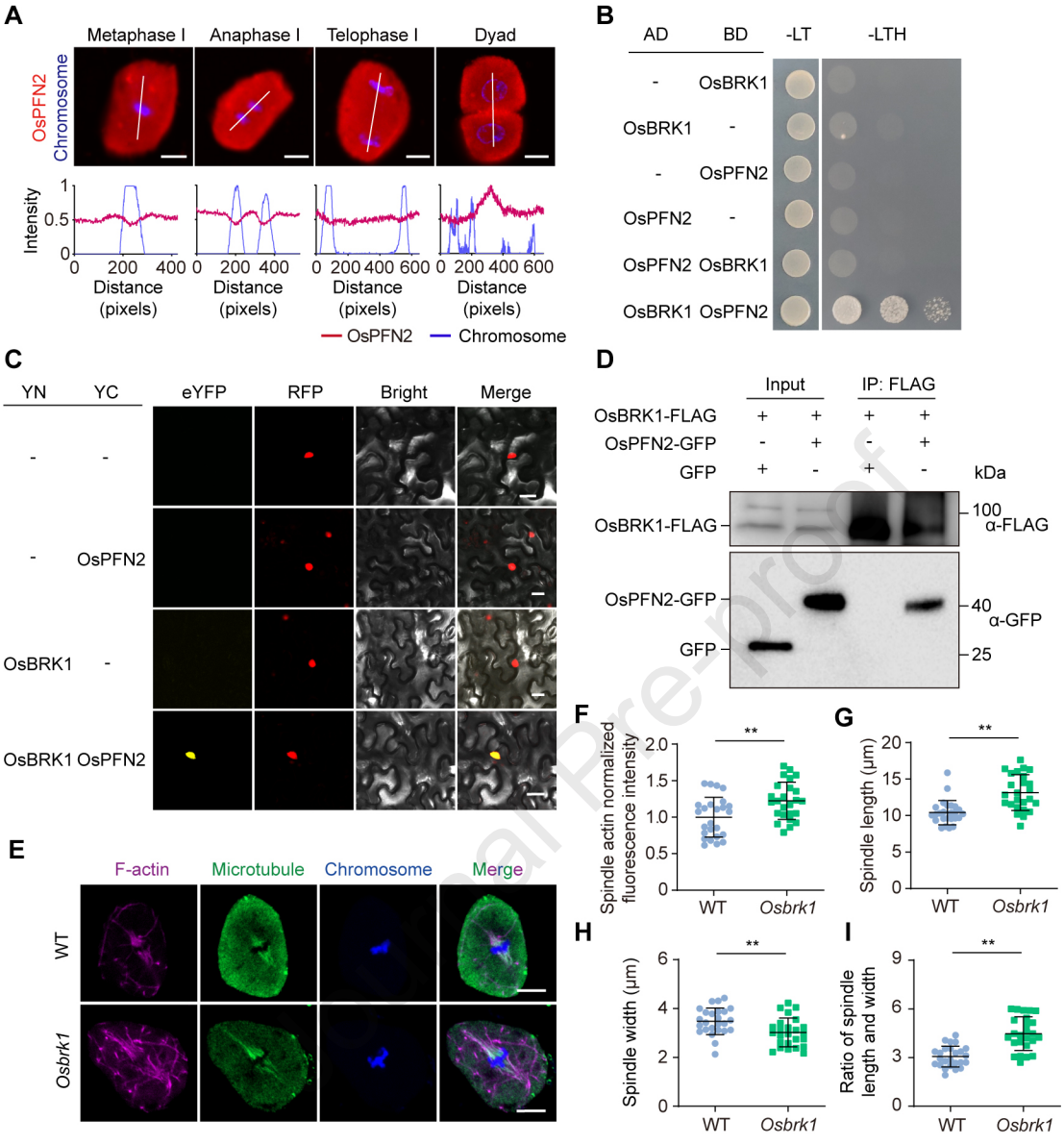

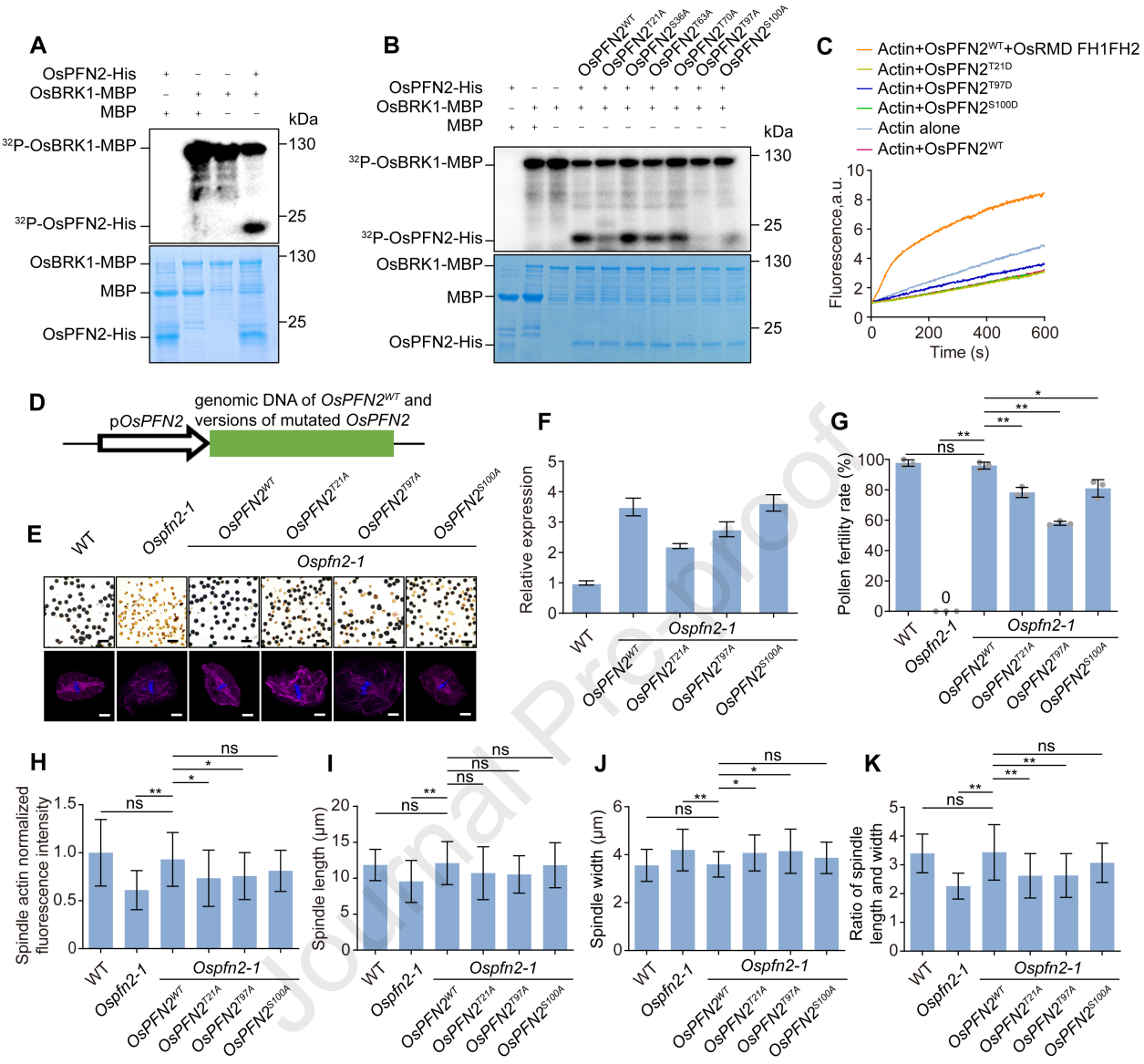

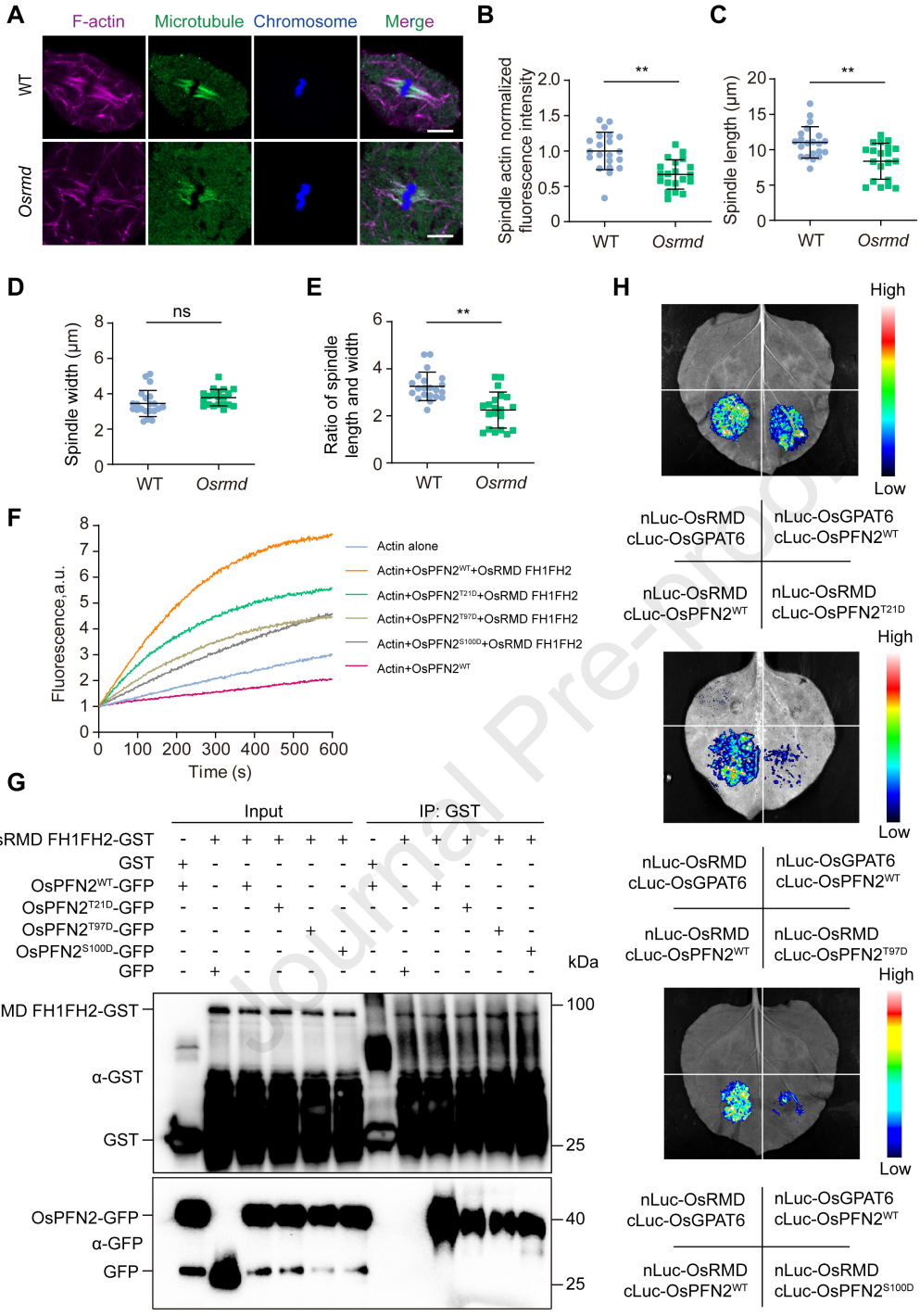
A
F-actin
Microtubule
Chromosome
Merge
WT
Osrmd
B
Spindle actin normalized fluorescence intensity
**
WT
Osrmd
C
Spindle length (μm)
**
WT
Osrmd
D
Spindle width (μm)
ns
WT
Osrmd
E
Ratio of spindle length and width
**
WT
Osrmd
F
Fluorescence,a.u.
Time (s)
Actin alone
Actin+OsPFN2WT+OsRMD FH1FH2
Actin+OsPFN2T21D+OsRMD FH1FH2
Actin+OsPFN2T97D+OsRMD FH1FH2
Actin+OsPFN2S100D+OsRMD FH1FH2
Actin+OsPFN2WT
G
Input
IP: GST
OsRMD FH1FH2-GST
GST
OsPFN2WT-GFP
OsPFN2T21D-GFP
OsPFN2T97D-GFP
OsPFN2S100D-GFP
GFP
kDa
α-GST
α-GFP
OsPFN2-GFP
H
High
Low
nLuc-OsRMD
cLuc-OsGPAT6
nLuc-OsGPAT6
cLuc-OsPFN2WT
cLuc-OsPFN2T21D
cLuc-OsPFN2T97D
cLuc-OsPFN2S100D